Turing patterns in an open reactor

John A. Vastano,[a] John E. Pearson,[a),b)] W. Horsthemke,[b)] and Harry L. Swinney[a)]
Department of Physics, University of Texas, Austin, Texas 78712

(Received 23 September 1987; accepted 3 February 1988)

Steady spatial chemical patterns have been found in model reaction–diffusion systems but have not yet been observed in any laboratory experiments. The reasons for this are discussed and the need for *open* reactors is stressed. A model open reactor is investigated in order to guide the experimental search for steady patterns. Specifically, Turing bifurcations in this reactor are studied for a simple autocatalytic chemistry (the Gray–Scott model) in order to determine the effects of varying diffusion coefficients, chemical time scales, and residence time. A description of all the steady-state bifurcations from an initially homogeneous state is obtained. The Liapunov–Schmidt reduction is used to determine the stability of the bifurcating solutions and a steady-state continuation technique is used to follow stable and unstable branches of bifurcating solutions.

I. INTRODUCTION

Turing's pioneering study *The Chemical Basis of Morphogenesis*[1] in 1952 established the theoretical possibility that reaction–diffusion systems could spontaneously form steady spatial patterns. He showed that a pattern or structure can develop due to an instability of the initially homogeneous steady state (HSS) as one or more parameters of the system are varied. The pattern arises spontaneously when a control parameter exceeds a critical value. Turing showed that the instability is a consequence of coupling between diffusion and chemical kinetics and that the pattern has an intrinsic "chemical wavelength" (Ref. 1, p. 51), i.e., a characteristic length that is *independent* of the boundary and initial conditions. In contrast, fluid flow patterns are not endowed with an intrinsic length; e.g., in Rayleigh–Bénard convection the wavelength of the convection rolls is determined by the thickness of the fluid layer.

Turing's ideas have been extended by Prigogine and Nicolis,[2,3] Haken,[4] Zhabotinskii and Zaikin,[5] Gierer and Meinhardt,[6] and others, and the theoretical literature now abounds with examples of time-*independent* chemical patterns. However, experiments thus far have revealed only time-*dependent* chemical patterns (propagating fronts, target patterns, spiral waves, etc.).[7–12] A few experiments have yielded time-independent patterns,[5,13–16] but those patterns apparently arose not from the interaction of reaction and diffusion but from fluid convection induced by evaporative cooling, double diffusive instabilities, or surface-driven instabilities.[13,17,18]

The main drawback of past experiments on chemical pattern formation is that they were conducted in closed systems, such as Petri dishes. Such systems inexorably relax to thermodynamic equilibrium. At or near equilibrium no spatial patterns can be formed; the Curie principle[19] forbids any coupling between reaction and diffusion. Further, experiments in closed systems lack a well-defined control parameter, such as the flow rate for a continuous flow stirred tank reactor (CSTR). This precludes the effective use of bifurcation theory, the primary tool in the analysis of nonlinear systems, to understand the experimental results. Both of these problems can be addressed by using reactors that are continuously fed so that the distance from thermodynamic equilibrium can be controlled. We call such a system a continuously fed unstirred reactor (CFUR). Noszticzius *et al.*[20] have built such a reactor in our laboratory.

In Sec. II we define Turing bifurcations and briefly discuss the Liapunov–Schmidt reduction, which we use to determine whether a given Turing bifurcation is supercritical or subcritical. In Sec. III we study Turing bifurcations for a simple model chemistry in an open reactor that is fed everywhere. In Sec. IV we summarize our results and comment on their relevance for experimental studies.

II. TURING BIFURCATIONS

Consider the steady state solutions to an n-species reaction–diffusion problem in a one-dimensional open reactor of finite length modeled by

$$\partial_t u = \mathbf{D}\partial_{zz} u + K(u) + \alpha(u_f - u) \tag{1}$$

with boundary conditions $(\partial u/\partial z|_{z=0,L} = 0)$ corresponding to impermeable ends. In Eq. (1), the t and z subscripts denote time and space derivatives, u is an n component vector of concentrations, $\mathbf{D}$ is the diagonal diffusion matrix, and $K(u)$ is a vector function of u representing the local mass-action kinetics. The last term on the right-hand side of Eq. (1) models a constant feed of chemicals through the reactor in a direction perpendicular to z; α is the inverse residence time and u_f is the vector of inlet feed concentrations; both are uniform over the extent of z. For Eq. (1) to be a valid model, this feed of chemicals must not impose any flow in the z direction. In experiments this can be realized by using reactors in which the reaction occurs in an inert gel.[20]

There may be several HSSs for Eq. (1), but the linear stability analysis proceeds in the same way for each of them. To simplify this analysis we use a change of variables to translate one HSS to zero. The model system then becomes

$$\partial_t u = \mathbf{D}\partial_{zz} u + \mathbf{A}u - F(u), \tag{2}$$

where $\mathbf{A}$ is a constant $n \times n$ matrix and F is an analytic vector function of u containing quadratic and higher-order terms.

[a)] Also in the Center for Nonlinear Dynamics, University of Texas.
[b)] Also in the Center for Studies in Statistical Mechanics, University of Texas.

 0021-9606/88/106175-07$02.10

The HSSs now correspond to solutions of the ordinary differential equation

$$\partial_t u = \mathbf{A}u - F(u) = 0, \tag{3}$$

which describes the (transformed) CSTR dynamics for the same model chemistry. (In the CSTR spatial inhomogeneities are removed by stirring and the diffusion is effectively infinite.) We are interested in the stability of the HSS corresponding to the $u = 0$ solution of Eq. (3) with respect to a perturbation $u(z,t)$. Although in the present work we consider only one-dimensional domains, the extension to higher-dimensional domains is straightforward for simple geometries.

We begin the stability analysis of the HSS by expanding $u(z,t)$ in terms of the eigenfunctions $\phi_k(z)$ of the operator ∂_{zz},

$$u(z,t) = \sum_k c_k(t)\phi_k(z), \tag{4}$$

where $c_k \in \mathbf{R}^n$ and k is the wave number, $k = m\pi/L$. Expansion (4) leads to the following set of equations for the c_k:

$$\frac{dc_k}{dt} = (\mathbf{A} - k^2\mathbf{D})c_k - \int_0^L F\left[\sum c_p(t)\phi_p(z)\right]\phi_k(z)dz. \tag{5}$$

The stability of the HSS is determined by the eigenvalues of the matrix $\mathbf{A} - k^2\mathbf{D}$. A Turing bifurcation occurs when a single eigenvalue of $\mathbf{A} - k^2\mathbf{D}$ crosses the imaginary axis (as a control parameter μ is varied) for some nonzero k in the spectrum of ∂_{zz}, while the real parts of all the eigenvalues of $\mathbf{A}$ remain negative. The matrix $\mathbf{A}$ determines the stability of the CSTR dynamics. Diffusion can destabilize the HSS if the rates of diffusive transport for the various species are sufficiently different. Conversely, if all the diffusion coefficients are equal, then diffusion cannot destabilize the HSS. However, this does not preclude pattern formation via finite amplitude inhomogeneous perturbations for systems with equal diffusion coefficients, as discussed by Vastano *et al.*[21]

To determine the bifurcation condition define

$$\Delta(k) \equiv \mathrm{DET}(\mathbf{A} - k^2\mathbf{D}). \tag{6}$$

For a Turing bifurcation to occur, the elements of $\mathbf{A}$ must depend upon a control parameter μ in such a way that $\Delta(k)$ has no real roots for $\mu < \mu_c$ and has two real roots for $\mu > \mu_c$. At $\mu = \mu_c$, $\Delta(k)$ has a double root, the critical wave number k_c; see Fig. 1. The fact that the bifurcation has a critical wave number that is independent of the system size has often been taken to imply that the resulting structures have an intrinsic length. This is strictly true only for infinite systems. In finite systems the critical wave number does not in general satisfy $k_c = m\pi/L$ for some integer m; hence it is necessary to go slightly beyond μ_c in order for the bifurcation to occur. The wave number of the bifurcating solution can differ from k_c by as much as π/L if k_c approaches zero.

By studying the linear stability of the HSS we thus obtain the wave number of the bifurcating eigenmode which destabilizes the HSS. If the bifurcation is supercritical the bifurcating solution is stable, and a pattern with the given wave number will grow from zero amplitude beyond the bifurcation. To determine the stability of the bifurcating solution we use the Liapunov–Schmidt reduction[22,23] to find the normal form of the bifurcation. An analysis of Turing bifurcations in a general reaction–diffusion setting will be contained in a forthcoming paper.[24] Here we will briefly review the reduction scheme and then state our results for the specific system (2). Given the bifurcation equation

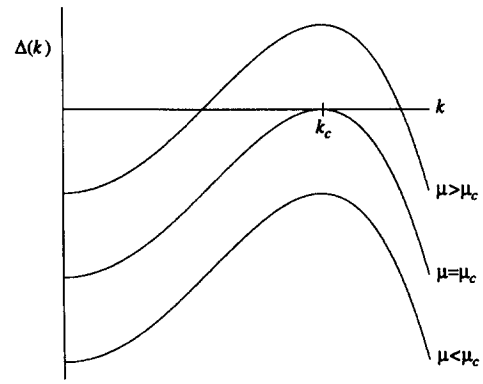

FIG. 1. Graphs of $\Delta(k)$, the determinant of the linear stability matrix for all wave number-k modes, for various values of the control parameter μ near a Turing bifurcation at $\mu = \mu_c$, for n odd [for n even, the sign of $\Delta(k)$ would be reversed].

$$\Psi(u,\mu) = \partial_t u - \mathbf{D}\partial_{zz}u - \mathbf{A}u + F(u) = 0 \tag{7}$$

or

$$\Psi = \Gamma u + F(u), \tag{8}$$

then, if $\Psi(0,0) = 0$ and Γ has a one-dimensional kernel (i.e., a single eigenmode becomes unstable), we can find a scalar function g satisfying

$$g(x,\mu) = 0 \tag{9}$$

whose solutions x are locally in one-to-one correspondence with solutions of $\Psi(u,\mu) = 0$. Roughly, x corresponds to the amplitude of the oscillations of the bifurcated solution, and g is the normal form of the bifurcation. It is not necessary to compute g explicitly; by computing the derivatives of g we can recognize the type of normal form and thus classify the bifurcation. For our model system we find that for all wave numbers m the Turing bifurcations have the form of a pitchfork bifurcation

$$g(x,\mu) = (\mu - \mu_c)x - \delta(\mu)x^3 + \cdots = 0. \tag{10}$$

Equation (10) has approximate solutions

$$x_s = 0, \tag{11a}$$

$$x_s = \pm\left[(\mu - \mu_c)/\delta\right]^{1/2}. \tag{11b}$$

If $\delta < 0$, then Eq. (11b) is unstable and the bifurcation is subcritical; if $\delta > 0$, the solution is stable and the bifurcation is supercritical.

III. TURING BIFURCATIONS IN A MODEL

To gain an understanding of the relevance of the various parameters in a CFUR, we have made a detailed study of the Turing bifurcations in our model CFUR (1) using a three-species reaction, an extension of the Schlögl model due to

Gray and Scott[25]:

$$A + 2B \underset{k'_{-1}}{\overset{k'_1}{\rightleftarrows}} 3B,$$

$$B \underset{k'_{-2}}{\overset{k'_2}{\rightleftarrows}} C.$$

The Gray–Scott model chemistry is well suited for our investigations for several reasons: first, it includes backreactions and thus can be brought close to thermodynamic equilibrium; second, it has no pool chemicals—this eliminates the need to maintain the (experimentally improbable) condition that those chemicals always remain in excess; third, since it has only three species, it is more amenable to analysis than larger models.

Consider the Gray–Scott model in our CFUR.[26] Chemicals are fed perpendicular to a thin reacting layer of length L. All species leave the reactor at the same rate α' and only species A is fed (at concentration A_0). The reaction–diffusion equation after transformation to nondimensional form is

$$\partial_t a = D_a \partial_{zz} a - ab^2 + \eta_1 b^3 + \alpha(1-a), \tag{12a}$$

$$\partial_t b = D_b \partial_{zz} b + ab^2 - \eta_1 b^3 - k_2(b - \eta_2 c) - \alpha b, \tag{12b}$$

$$\partial_t c = D_c \partial_{zz} c + k_2(b - \eta_2 c) - \alpha c \tag{12c}$$

with no-flux boundary conditions at $z' = 0$ and $z' = L$ (primes indicate the original, dimensioned variables); $a = A/A_0$, $b = B/A_0$, $c = C/A_0$, $t = t' k'_1 A_0^2$, $k_2 = k'_2/A_0^2 k'_1$, $\alpha = \alpha'/k'_1 A_0^2$, $\eta_1 = k_{-1}/k_1$, $\eta_2 = k_{-2}/k_2$, $z = z'/L$, *and* $D_i = D'_i/k'_1 A_0^2 L^2$ $(i = a,b,c)$.

Our investigations were made with $L = 0.204$ cm, $k_1 A_0^2 = 1\,s^{-1}$, and $D'_b = D'_c = 10^{-5}$ cm^2/s. We leave k_2, α, and D_a $(D_a > 0)$ as free parameters. We have found that the strength of the backreactions has little effect on our results, and the work reported here was done with $\eta_1 = \eta_2 = 10^{-2}$.

We briefly discuss the Gray–Scott model in a CSTR in order to provide a reference point.[25] The trivial steady state in a CSTR ($a = 1$, $b = c = 0$) is stable at all feed rates and chemical time scales. In the region of the $\alpha - k_2$ plane shown in Fig. 2(a) the model has bistability. The stable nontrivial steady state and an unstable steady state comprise an isola as α is varied for a fixed value of k_2; an example is shown in Fig. 2(b). The stable nontrivial steady state loses stability by a saddle-node bifurcation (at large α) or a Hopf bifurcation (at small α). The Hopf bifurcation on the upper branch of the isola may be subcritical or supercritical, depending on the rate constant k_2.

The reaction–diffusion system [Eq. (12)] has a HSS corresponding to any steady state in the CSTR model. We

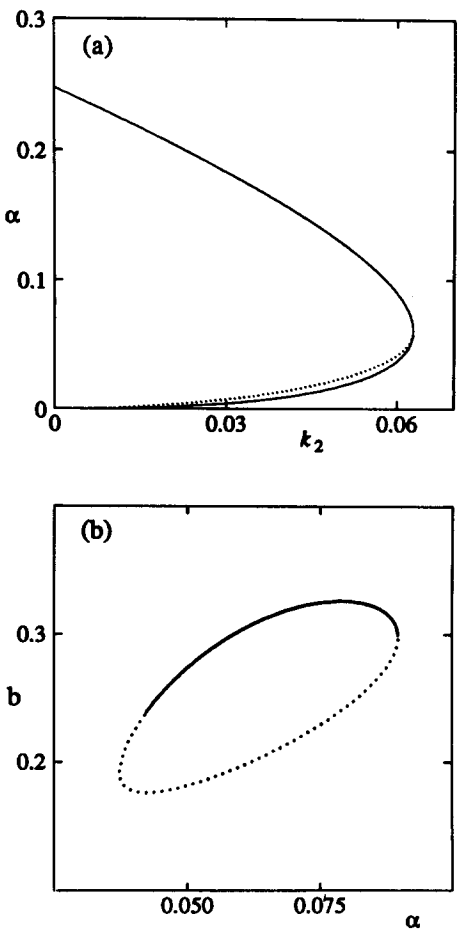

FIG. 2. (a) The nontrivial steady states of the CSTR exist within the region bounded by the solid curve. The stable nontrivial steady state becomes unstable via a saddle-node bifurcation at high α and via a Hopf bifurcation at low α. The dotted curve indicates the Hopf bifurcations, which are supercritical for $k_2 < 0.0368$, subcritical for $k_2 > 0.0368$. (b) The isola of nontrivial steady states for the CSTR is shown for fixed $k_2 = 0.06$. The solid curve indicates stable steady states; the dotted curve, unstable steady states.

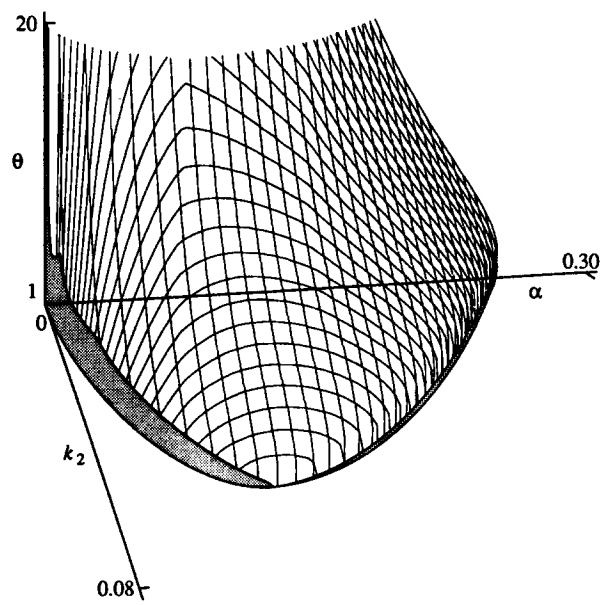

FIG. 3. The critical surface for Turing bifurcations for a ratio of diffusion coefficients in the range $1 < \theta < 20$. The surface is bounded at low α by the line of CSTR Hopf bifurcations and at high α by the line of CSTR saddle-node bifurcations. As an aid to the eye, these boundaries are marked by shaded surfaces which are normal to the $\alpha - k_2$ plane. If the system passes through the critical surface as a parameter is tuned, it undergoes a Turing bifurcation. If the system passes through one of the normal surfaces, it undergoes either a homogeneous Hopf (at low α) or homogeneous saddle-node bifurcation (at high α).

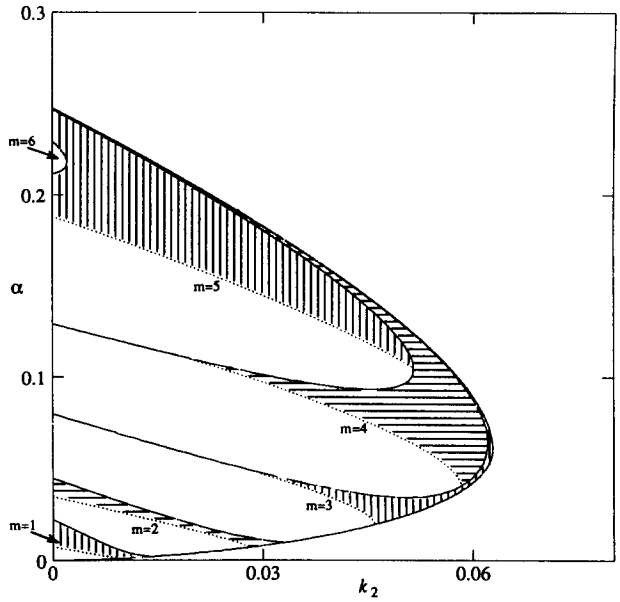

FIG. 4. A projection of the critical surface (Fig. 3) onto the α–k_2 plane, showing the wave number of the Turing bifurcation and the stability of the bifurcating solution. The region is bounded at high α by the line of homogeneous saddle-node bifurcations and at low α by the line of homogeneous Hopf bifurcations. For each wave number a dotted line separates the region of subcritical Turing bifurcations (hatched region) from the region of supercritical Turing bifurcations.

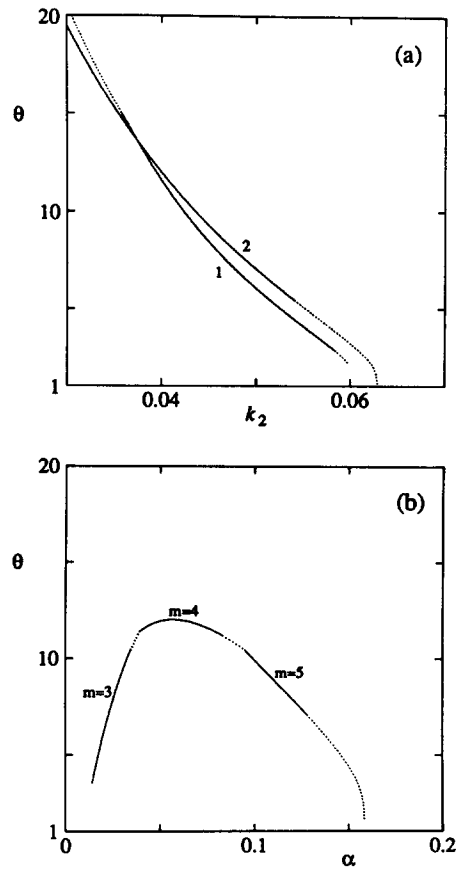

FIG. 5. Sections of the surface of Turing bifurcations. Solid lines denote supercritical Turing bifurcations; dashed lines, subcritical Turing bifurcations. (a) Sections for α fixed and k_2 varied: curve 1, $\alpha = 0.0415$; curve 2, $\alpha = 0.0628$. Curve 1 becomes supercritical at $k_2 = 0.0583$, $\theta = 2.82$. This is the minimum value of θ for a supercritical Turing bifurcation in this system. For curve 2 subcritical bifurcations occur for θ arbitrarily close to one. (b) A section with α varied and k_2 fixed ($k_2 = 0.04$). As α is increased for a given wave number, the Turing bifurcation changes from supercritical to subcritical before changing to the next wave number (cf. Fig. 4).

seek Turing bifurcations off the (stable) nontrivial HSS. In addition to the two free parameters (α and k_2) from the CSTR dynamics, we have as a parameter the ratio of diffusion coefficients $\theta = D_a/D_b$ (there is only a weak dependence on the ratio D_c/D_b, and we set $D_b = D_c$). To locate the bifurcations, let θ be a free parameter, set the determinant in Eq. (6) to zero and solve for θ as a function of α, k_2, and wave number ($m\pi/L$, $m = 1,2,...$; henceforth we shall refer to m as the wave number). This yields a different value of θ for each m; the bifurcation occurs at the smallest positive value of θ. The critical surface is given by

$$\theta_c(\alpha,k_2) \equiv \min_m \theta(\alpha,k_2,m), \tag{13}$$

which is defined in the region of the $\alpha - k_2$ plane for which there exists a stable nontrivial steady state in the local dynamics. Part of the critical surface is shown in Fig. 3. If θ is fixed and k_2 or α is varied, there are two ways to leave the region beneath this surface: by passing through the surface and undergoing a Turing bifurcation, or by passing below the surface and undergoing a homogeneous ($k = 0$) bifurcation. The homogeneous bifurcation is either a Hopf or a saddle-node bifurcation, depending on α and k_2.

Both subcritical and supercritical Turing bifurcations occur in the CFUR. Figure 4 is a projection of the critical surface onto the $\alpha - k_2$ plane, showing the wave number of the bifurcation as a function of those two parameters and indicating the stability of the bifurcating pattern, determined by computing the Liapunov–Schmidt reduction of the bifurcation. The smallest θ for which supercritical bifurcations occur is approximately 2.8, while subcritical bifurcations occur for θ arbitrarily close to unity.[24] In Fig. 5(a) two sections of the critical surface are shown by varying k_2 for two fixed values of α. The first section passes through the point on the critical surface where the minimum value of θ necessary for a supercritical bifurcation is attained. However, there is only a small range of k_2 for which θ is near 2.8. The second section passes through the tip of the region of CSTR bistability in $\alpha - k_2$ parameter space, where θ approaches unity for subcritical Turing bifurcations. Typically, as α is increased away from the homogeneous Hopf bifurcation, bifurcations of a given wave number change from supercritical to subcritical. This is illustrated in Fig. 5(b).

To model the reaction–diffusion problem (12), we discretize the spatial variable with a grid of 50 sites and use second-order centered differencing of the chemical concentrations at the grid points to model the spatial derivatives. Since there are three independent chemical species and 50 grid points, we obtain a set of 150 coupled ordinary differential equations as a discretized model of Eq. (12). The applicability of results from this discretized model to steady states of the partial differential equation (12) obviously depends on the number of spatial grid points used. Tests using 30, 50,

150, 250, and 500 grid points have revealed no substantive differences.

Some of the bifurcations that we study are subcritical; therefore, it is necessary to follow curves of unstable steady-state solutions. We accomplish this by using a steady-state continuation technique on the system of coupled equations. The object of steady-state continuation is to follow a curve of steady states as some system parameter, e.g., the feed rate α, is varied. We use a predictor–corrector technique: two steady states at slightly different values of the parameter are used to predict the steady state at some new value by linear extrapolation. Newton–Raphson iteration then corrects the prediction and returns the solution to the curve of steady states. The corrector converges to the "nearest" solution, whether it is stable or unstable. Thus by exercising caution in the step size chosen we can trace out any curve of steady-state solutions, once we find a starting point along it. We determine the linear stability of the new solution by computing the eigenvalues of the discretized system linearized about the solution. To follow a bifurcating solution off a given curve of states at a change in stability, we add a small multiple of the newly unstable eigenvector to the current state and then use Newton–Raphson iteration to adjust for any nonlinear effects. We can thus systematically find and follow any curve of steady states connected to the HSS, as any system parameter is varied.

In Fig. 6 we present diagrams for a typical supercritical Turing bifurcation as a function of α with fixed θ and k_2. The form of the critical surface in $\alpha - k_2 - \theta$ parameter space can be seen in Fig. 3: for fixed k_2 and θ there is a region at moderate values of α in which the HSS is stable (on the upper branch of the isola). Increasing or decreasing α takes the system across the critical surface, and the HSS becomes unstable to a given wave number perturbation. In the present case, the HSS is stable over the range $0.051 < \alpha < 0.063$. As α is tuned past either end of the interval, the system undergoes a supercritical wave number-4 bifurcation. In Fig. 6(a) we display the further evolution with α of the bifurcated wave number-4 pattern. At high α the pattern loses stability in a saddle-node bifurcation, while at low α it undergoes a subcritical Hopf bifurcation. Note that a stable pattern persists well outside the region of CSTR parameter $(\alpha - k_2)$ space in which there is nontrivial behavior. (Outside the region of bistability in the CSTR, indicated by the isola of HSS, there is only the trivial solution, $b = 0$.) Thus, finite and unequal diffusion coefficients allow pattern formation in regions of parameter space in which no nontrivial states are possible in the well-mixed system.

After the wave number-4 Turing bifurcation, several other solutions bifurcate from the HSS as other eigenfunctions become unstable. For the sake of clarity we will display only those branches that contain *stable* patterns. The second bifurcating pattern shown in Fig.6(a) arises from a wave number-5 bifurcation. The solution bifurcates from the upper branch of the HSS isola as an unstable pattern, later stabilizes, and then undergoes a saddle-node bifurcation leading back to a bifurcation point on the lower branch of the HSS isola.

There are two other branches off the HSS which contain stable patterns, and these are depicted in Fig. 6(b). The wave number-6 branch behaves much as does the wave number-5 branch, bifurcating off the upper branch of the isola, stabilizing, undergoing a saddle-node bifurcation, and reattaching to the HSS on the lower branch of the isola. The wave number-3 solution, however, displays a different bifurcation sequence. It bifurcates off the upper branch of the HSS isola in the low α regime, subsequently stabilizes, loses stability in a Hopf bifurcation, and then undergoes two saddle-node bifurcations, first at low α and then at high α. At this point the pattern becomes stable again. The curve eventually reattaches, not to the isola of HSS, but to the curve of wave number-6 patterns.

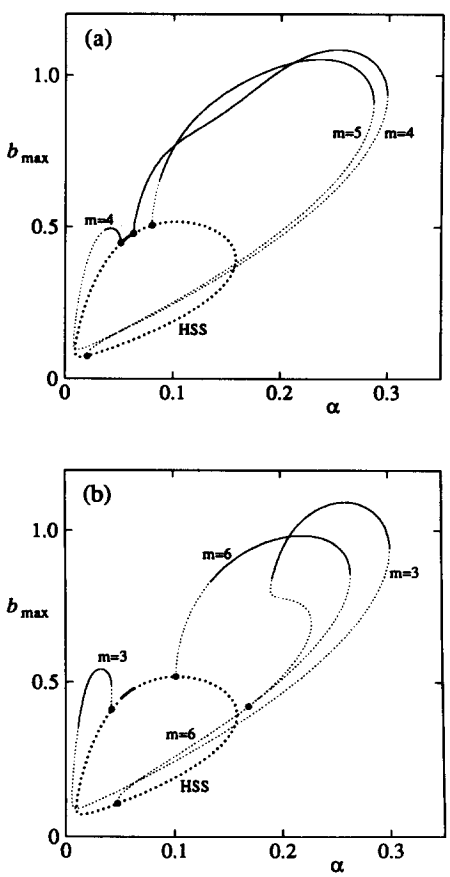

FIG. 6. Supercritical Turing bifurcations, for $\theta = 11.95$ and $k_2 = 0.04$. For clarity the solutions bifurcating from the HSS are shown separately for wave numbers 4 and 5 in (a) and 3 and 6 in (b). The ordinate is the maximum value of b as it varies spatially on a waveform. Solid lines indicate stable patterns; dotted lines, unstable patterns. A bold solid line indicates a stable HSS; a bold dotted line, an unstable HSS. Points where curves actually intersect are marked by large dots.

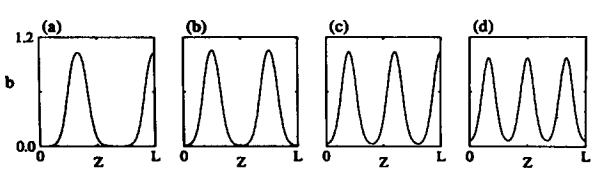

FIG. 7. Stable patterns with wave numbers (a) 3, (b) 4, (c) 5, and (d) 6, observed at $\theta = 11.95$, $k_2 = 0.04$, and $\alpha = 0.22$ (cf. Fig. 6).

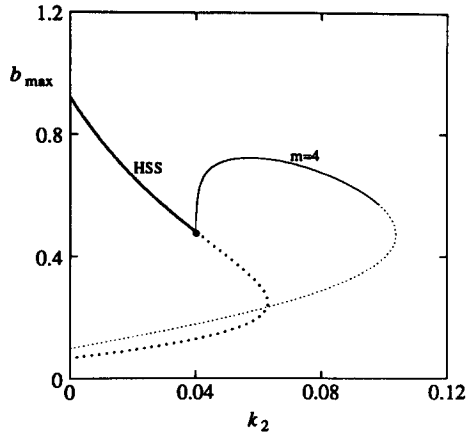

FIG. 8. Supercritical Turing bifurcation, for $\theta = 11.95$ and $\alpha = 0.063$. Only the wave number-4 bifurcation is shown. The conventions for the lines are the same as in Fig. 6.

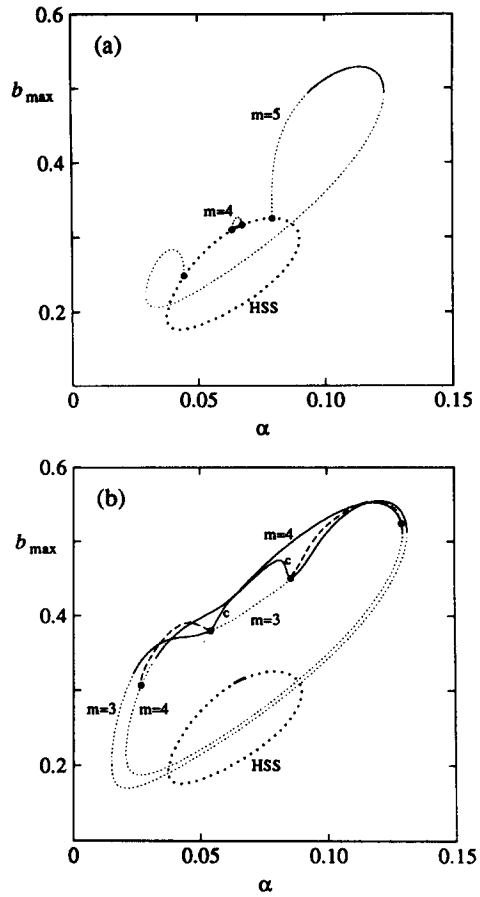

FIG. 9. Subcritical Turing bifurcations for $\theta = 3.2$ and $k_2 = 0.06$. Curves of solutions connected to the HSS are shown in (a), while solution curves which are disconnected from the HSS at this value of k_2 are shown in (b). The conventions for the lines are those of Fig. 6, with one addition: the dashed curves in (b) indicate the unstable portions of a curve of solutions connecting the two isolas. This connecting curve consists of stable patterns over the range of α where the wave number-3 isola consists of unstable patterns: that section of the curve is identified by the small letter "c." In (a), the curves are identified by the wave number of the bifurcating solution off the HSS. In (b), the isolas are identified by their connection to the HSS found by varying k_2 (cf. Fig. 11).

Although we identify the curves by the wave number of the bifurcation off the HSS which gives rise to them, the patterns evolve with changing α and can look quite different from the pure cosine function of the perturbation. At the point where it bifurcates from the curve of wave number-6 patterns, the wave number-3 curve consists of patterns that are essentially wave number 6. However, it is usually possible to discern the wave number of the original bifurcation in the stable patterns. There is a range of feed rates $0.20 < \alpha < 0.26$ in which there are four stable nontrivial patterns for this $k_2 - \theta$ setting, as shown for $\alpha = 0.22$ in Fig. 7. Wave numbers 3 through 6 are clearly identifiable.

At the bifurcation the sign of the perturbation is unimportant. However, at finite distance from the bifurcation the solutions corresponding to the different signs are not necessarily identical. In our system, the difference between the two solutions is less than 0.1%, and we have therefore plotted only the curves of solutions arising from perturbations with $\phi_k(x = 0) < 0$.

Rather than fixing k_2 and varying α, we can fix α and investigate the curve of solutions as k_2 varies; this is shown in Fig. 8. For the sake of clarity we show only the wave number-4 curve of steady states. Again, notice that the region of stability for the pattern extends beyond the region of nontrivial behavior in the CSTR.

Figure 9 is the bifurcation diagram for a typical subcritical Turing bifurcation, again of wave number 4. The HSS is stable over the range $0.0634 < \alpha < 0.067$. Notice in Fig. 9(a) that the subcritical bifurcation apparently results only in a small closed curve of unstable solutions. As in the case of the supercritical bifurcation, a number of other bifurcations off the HSS occur as other wave numbers become unstable. The wave number-5 solution curve is the only one which bifurcates off the HSS and stabilizes, and it does so in a regime of α away from the region of the isola of HSS. The most important patterns observed in the system, the ones that appear spontaneously as α is increased (or decreased) from the region of HSS stability, are isolas of large amplitude patterns. These are shown in Fig. 9(b). There are two isolas of steady-state patterns, and a connecting curve of patterns between them. The connecting curve bifurcates from the wave number-4 isola at low α, connects to the wave number-3 isola twice at intermediate α, and then returns to the wave number-4 isola at high α. In the range of α between its connec-

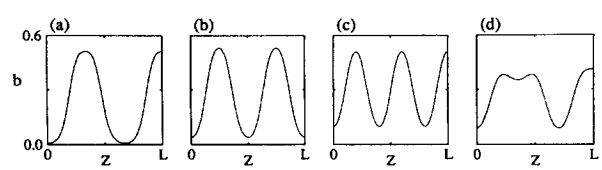

FIG. 10. Stable patterns observed at $\theta = 3.2$ and $k_2 = 0.06$. In (a), (b), and (c), $\alpha = 0.1$; in (d), $\alpha = 0.07$. Each pattern corresponds to one of the curves of steady states in Fig. 9. The wave number-3 and 4 patterns corresponding to the isolas of Fig. 9(b) are shown in (a) and (b), and the wave number-5 pattern on the curve bifurcating from the HSS isola in Fig. 9(a) is shown in (c). The stable steady state found on the curve connecting the wave number-3 and wave number-4 isolas of Fig. 9(b) at $\alpha = 0.07$ is shown in (d).

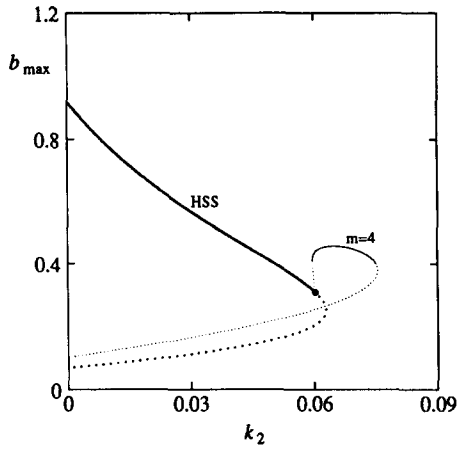

FIG. 11. Subcritical Turing bifurcation for $\theta = 3.2$ and $\alpha = 0.063$. Only the wave number-4 bifurcation is shown. The conventions for the lines are those of Fig. 6.

tions to the wave number-3 isola, the patterns on this curve are stable while the patterns on the wave number-3 isola are unstable. The stable patterns on the connecting curve resemble a wave number-3 pattern.

Patterns on the isolas, as seen in Fig. 10, are wave number-3 and 4 states, but they do not appear to bifurcate from the HSS. This is explained in Fig. 11, which traces a solution curve from the wave number-4 isola. The isola observed by varying α at fixed $k_2 = 0.06$ is seen to be connected to the HSS at $k_2 = 0.058$; notice also that the curve of unstable wave number-4 patterns from the Turing bifurcation as α is varied appears in cross section as part of the unstable branch leading to a saddle node where the pattern stabilizes. The wave number-3 isola can also be traced back to the HSS by varying k_2. We have not been able to find any nontrivial steady-state solution that cannot be traced to a bifurcation from the HSS by varying α or k_2. This is not a guarantee that such states do not exist, but if they do they are difficult to find and are likely unstable.

IV. CONCLUSIONS

There has not yet been any experimental corroboration of Turing's well-known theory of stationary pattern formation in chemical reaction–diffusion systems. We suggest that the use of continuously fed unstirred reactors (CFURs) should make it possible to observe Turing bifurcations in laboratory experiments.

The observation of a steady chemical pattern in such a reactor would not by itself qualify as a convincing demonstration of a Turing bifurcation. It is necessary to observe the destabilization of a HSS as some parameter is increased, and the growth from zero amplitude of the bifurcating steady pattern. This demands that the bifurcation be supercritical. In our model system, supercritical Turing bifurcations occurred only for a ratio of diffusion coefficients of at least 2.8, while subcritical Turing bifurcations were found to occur for ratios of diffusion coefficients arbitrarily near unity. This suggests that in experimental systems involving species with nearly equal diffusion coefficients, the bifurcations leading to steady pattern formation will be either subcritical Turing bifurcations or the bifurcations from the unstable HSS that we reported previously.[21] However, supercritical Turing bifurcations should be observable in experimental systems involving species with widely different diffusion coefficients, e.g., reaction schemes involving immobilized catalysts in a gel.

Our investigations using a steady-state continuation technique to trace bifurcating solutions off the HSS have uncovered a complicated bifurcation structure with several stable patterns coexisting for large ranges of system parameters. Stable steady patterns were found to exist in regions of parameter space where the homogeneous dynamics could produce only trivial steady states. This is an encouraging indication that the regions of experimental parameter space over which interesting steady state patterns will be found should not be too small.

ACKNOWLEDGMENTS

We thank John Ringland for advice on steady-state continuation techniques. The computations were performed at the University of Texas Center for High Performance Computing. This work was supported by grants from the Venture Research Unit of British Petroleum and the Department of Energy Office of Basic Energy Sciences.

[1] A. M. Turing, Philos. Trans. R. Soc. London Ser. B **237**, 37 (1952).
[2] I. Prigogine and G. Nicolis, J. Chem. Phys. **46**, 3542 (1967).
[3] G. Nicolis and I. Prigogine, *Self-Organization in Nonequilibrium Systems* (Wiley, New York, 1977).
[4] H. Haken, *Synergetics* (Springer, Berlin, 1977).
[5] A. M. Zhabotinskii and A. N. Zaikin, J. Theor. Biol. **40**, 45 (1973).
[6] A. Gierer and H. Meinhardt, Kybernetik **12**, 30 (1972).
[7] A. N. Zaikin and A. M. Zhabotinskii, Nature **225**, 535 (1970).
[8] A. T. Winfree, Science **175**, 634 (1972).
[9] M. Marek and E. Svobodova, Biophys. Chem. **3**, 263 (1975).
[10] M. L. Smoes, in *Dynamics of Synergetic Systems*, edited by H. Haken (Springer, Berlin, 1980), p. 80.
[11] P. M. Wood and J. Ross, J. Chem. Phys. **82**, 1924 (1985).
[12] S. C. Müller, T. Plesser, and B. Hess, Science **230**, 661 (1985).
[13] K. Showalter, J. Chem. Phys. **73**, 3735 (1980).
[14] M. Orban, J. Am. Chem. Soc. **102**, 4311 (1980).
[15] P. Möckel, Naturwiss. **64**, 224 (1977).
[16] M. Kagan, A. Levi, and D. Avnir, Naturwiss. **69**, 548 (1982); D. Avnir and M. Kagan, Nature **307**, 717 (1984).
[17] J. C. Micheau, M. Gimenez, P. Borckmans, and G. Dewel, Nature **305**, 43 (1983).
[18] P. Borckmans, G. Dewel, D. Walgraef, and Y. Katayama, J. Stat. Phys. **48**, 1031 (1987).
[19] S. R. deGroot and P. Mazur, *Non-Equilibrium Thermodynamics* (Dover, New York, 1985), p. 57.
[20] Z. Noszticzius, W. Horsthemke, W. D. McCormick, H. L. Swinney, and W. Y. Tam, Nature **329**, 619 (1987); W. Y. Tam, W. Horsthemke, Z. Noszticzius, and H. L. Swinney, J. Chem. Phys. **88**, 3395 (1988).
[21] J. A. Vastano, J. E. Pearson, W. Horsthemke, and H. L. Swinney, Phys. Lett. A **124**, 320 (1987).
[22] M. Golubitsky and D. Schaeffer, *Singularities and Groups in Bifurcation Theory* (Springer, New York, 1985).
[23] J. F. G. Auchmuty and G. Nicolis, Bull. Math. Biol. **37**, 323 (1975).
[24] J. E. Pearson and W. Horsthemke (to be published).
[25] P. Gray and S. K. Scott, Chem. Eng. Sci. **38**, 29 (1983); **39**, 1087 (1984); J. Phys. Chem. **89**, 22 (1985).
[26] S. K. Scott, Chem. Eng. Sci. **42**, 307 (1987). In this paper, the Gray–Scott model chemistry is considered in a reaction–diffusion setting, but there is no global feed of chemicals, so a HSS is not possible, and the diffusion coefficients are held equal, so there is no destabilizing mechanism that could give rise to a Turing bifurcation.